J. S. Afr. Inst. Min. Metall., vol. 91, no. 11.
Nov. 1991. pp. 397–409.

The reduction of chromite in liquid iron–chromium–carbon alloys

by E. USLU* and R.H. ERIC†

SYNOPSIS

The kinetics of the reduction of chromite from the LG-6 layer of the Bushveld Complex in Fe–Cr–C alloys were studied in the temperature range 1500°C to 1680°C under an inert argon atmosphere. The rotating cylinder technique was used, and the rotational speed of the chromite cylinder ranged from 0 to 1000 r/min. The melt consisted of 30 to 80 per cent chromium and 2 to 8 per cent carbon. The initial chromium-to-iron ratios of the melts varied between 0,42 and 4,95. The reduction of chromite spinel was analysed in terms of the decarburization of the metal.

It was found that decarburization increased with an increase in the temperature, the carbon content of the bath, and the rotational speed of the cylinder up to 400 r/min, after which it remained almost constant. Decarburization also increased with an increase in the chromium content up to about 50 per cent chromium but, at higher chromium contents, it decreased. In the early stage of the reduction, up to about 30 minutes of reaction time, the liquid-state mass transfer of oxygen was found to be the most likely rate-determining step. The apparent activation energy was calculated to be 84,864 kJ per mole of oxygen. In the later stage, diffusion of iron and/or chromium in the solid state is the most likely rate-determining step. The apparent activation energy for the diffusion was calculated to be 471,18 kJ/mol.

SAMEVATTING

Die kinetika van die reduksie van chromiet afkomstig van die LG6-laag van die Bosveldkompleks in Fe-Cr-C-legerings is in die temperatuurstrek 1500°C tot 1680°C onder 'n trae argonatmosfeer bestudeer. Die draaisilindertegniek is gebruik en die draaispoed van die chromietsilinder het gewissel van 10 tot 1000 r/min. Die smeltsel het bestaan uit 30 tot 80 persent chroom en 2 tot 8 persent koolstof. Die aanvanklike chroomysterverhoudings van die smeltsels het gewissel tussen 0,42 en 4,95. Die reduksie van chromietspinel is in terme van die dekarburisering van die metaal ontleed.

Daar is gevind dat die dekarburisering toegeneem het met 'n styging in die temperatuur, die koolstofinhoud van die bad, en die draaispoed van die silinder tot 400 r/min, waarna dit feitlik konstant gebly het. Die dekarburisering het ook toegeneem met 'n verhoging van die chroominhoud tot ongeveer 50 persent chroom maar met 'n hoër chroominhoud het dit afgeneem. In die vroeë stadium van die reduksie, tot ongeveer 30 minute van die reaksietyd, is daar gevind dat die massaoordrag van suurstof in die vloeibare toestand die waarskynlikste tempobepalende stap is. Die skynbare aktiveringsenergie is bereken as 84,864 kJ per mol suurstof. In die later stadium is diffusie van yster en/of chroom in die vaste toestand die waarskynlikste tempobepalende stap. Die skynbare aktiveringsenergie vir die diffusie is bereken as 471,18 kJ/mol.

Introduction

In the past, a number of investigations[1–6] have been undertaken on the solid-state reduction of chromites from the Bushveld Complex of the Transvaal. Although the mechanism and kinetics of the reduction of these chromites by carbon have already been studied[4-6], the possibility of direct stainless steel production by the use of ores containing chromium and iron is attracting more and more attention. Systematic fundamental studies on the kinetics and mechanism involved in the reduction of chromites by liquid Fe–Cr–C alloys are therefore necessary.

A major shift in the grades of ferrochromium produced took place in the early 1970s, resulting in an increase in the production of high-carbon ferrochromium and a decrease in the production of low-carbon ferrochromium. This change took place as a result of the introduction of the argon–oxygen decarburization (AOD) process, which makes it possible for the carbon content of a melt to be reduced to the amount required for the production of stainless steel with the minimum oxidation of the chromium.

In the AOD process, the injected oxygen oxidizes the molten iron, the dissolved chromium, and the dissolved carbon around the tuyères. The formed iron and chromium oxides are subsequently reduced by the carbon in the melt, resulting in the selective oxidation of the carbon. In the direct production of stainless steel from chromium ore, the available oxygen in the form of iron and chromium oxides could possibly be used, in addition to gaseous oxygen, to oxidize the carbon. Studies of such a possibility are also relevant to the refining of ferrochromium.

A knowledge of the rate-controlling mechanism and the kinetics of the reduction of chromite spinels by carbon dissolved in Fe–Cr alloys is important in the development of a technology that will minimize chromium loss and enhance decarburization of the melt in the production of ferrochromium and stainless steel.

This paper describes a study of the kinetics of the reduction of chromite with the idealized formula $FeO.Cr_2O_3$ or $FeCr_2O_4$, i.e.

$$FeCr_2O_4(s) + C = Fe\ (l) + 2\ Cr\ (l) + 4\ CO(g)\ , \qquad [1]$$

* Highveld Steel & Vanadium, P.O. Box 111, Witbank, 1035 Transvaal.
† University of the Witwatersrand, P.O. Wits, 2050 Transvaal.
 SA ISSN 0038–223X/3.00 + 0.00. Paper received 12th June, 1990; modified paper received 25th March, 1991.

where s = solid phase
l = liquid phase
g = gas phase.

Equation [1] does not represent the mechanism of the reaction, which consists of a series of steps involving chemical reaction and the transportation of reactants and products to and from the reaction sites. The object of the study was to determine a probable mechanism for the reduction of chromite spinels by carbon dissolved in Fe–Cr alloys, and to determine which step controls the rate of the overall reaction.

The various steps comprising a reaction can be differentiated when the rate of each step is varied by systematic changes in the variables affecting that particular step. It is therefore necessary to know, quantitatively, the effect that each of several variables will have on the rate of each step.

Because mass-transport steps are influenced by the hydrodynamics of the system under consideration, it is most desirable to have a system for kinetic study that has well-defined hydraulic–hydrodynamic conditions. Since the mass-transfer characteristics of rotating cylinders are already known, the method chosen for this study involved rotating chromite spinel cylinders in liquid Fe–Cr–C alloys.

This study, in a broad sense, concerns the general class of reactions between solid oxides, molten metal, and gas. Specifically, the study is relevant to the use of chromium ore as a decarburizing and chromium-supplying agent.

Experimental Procedure

The chromite-spinel cylinders were prepared from pulverized LG-6 chromite fines (Table I), which had been treated on a shaking table for the removal of clay minerals and sand. The duration of pulverization was 2 minutes, and the powder was formed into dry cylinders without any binders by uniaxial pressing in a steel mould under a pressure of 8 t. This was followed by sintering under argon gas flowing at a rate of 400 cm³/min at 1400°C for 3 hours in a molybdenum-wound furnace with a recrystallized-alumina work tube. Care was taken that the sintered cylinders were free of cracks.

Table II lists the chemical composition of the chromite from LG-6 fines of the Bushveld Complex. The number of moles of cations per 32 moles of oxygen (calculated from mass percentage of the sintered chromite) gave the following chemical formula for this chromite: $(Fe_{4,03}, Mg_{3,97})$ $[Cr_{10,01}, Al_{4,29}, Fe^{3+}{}_{1,48}, Fe^{2+}{}_{0,11}, Ti^{4+}{}_{0,11}]$ O_{32}, where round and square brackets represent tetrahedral and octahedral sites respectively. This formula is in reasonably good agreement with the result obtained by De Waal and Hiemstra[7].

The metallic furnace charges were premelted Fe–Cr–C alloys, together with the necessary additions of spectroscopic-grade graphite and laboratory reagent-grade iron and chromium powders. Two master alloys were prepared from electrolytic iron, electrolytic chromium, and spectroscopic graphite in a vacuum-induction furnace. Chemical analyses of the master alloys are given in Table III.

The reduction furnace illustrated in Fig. 1 was heated by a stable 50 kW 3 kHz induction unit. The furnace chamber consists of a fused-silica tube, 50 cm long, with an outside diameter of 12 cm and an internal diameter of 11,4 cm. The lower end of the tube was closed, and the top was closed by a water-cooled brass plate. An O-ring between the silica tube and the brass plate ensured gas-tightness.

A dense-graphite crucible was used as the heating element, in which the alumina crucible, 68 cm long and with an internal diameter of 47 mm, was placed. A graphite cover was used as a radiation shield. The space between the graphite crucible and the outer silica tube, as well as the bottom section of the silica tube, was packed with lampblack for insulation.

Considerable care was devoted to the design and construction of the system, so that a uniform temperature could be maintained within the alumina crucible.

Measurements using a Pt–6%Rh/Pt–30%Rh thermocouple showed that the temperature in the region from the bottom of the crucible to the top varied by no more than 2°C. Because of the stability of the induction furnace, it was seldom necessary to make adjustments to the power setting after the initial adjustment had been made. It is estimated that the temperature of the system during a run did not vary by more than about 10°C from the initial setting.

The furnace assembly was gas-tight and, during the experiments, the pressure in the system was slightly above the ambient atmospheric pressure. An inert argon atmosphere was maintained within the furnace chamber. The flowrate of the gas, measured with a capillary flowmeter, was supplied to the furnace at a rate of 2000 cm³/min. Before entering the system, the gas was dried in a drying chamber filled with anhydrous $Mg(ClO_4)_2$ as a desiccant, as well as silica gel. The gas then entered a deoxidation furnace containing copper chips, which were maintained at 500°C. The gas was introduced into the reaction chamber

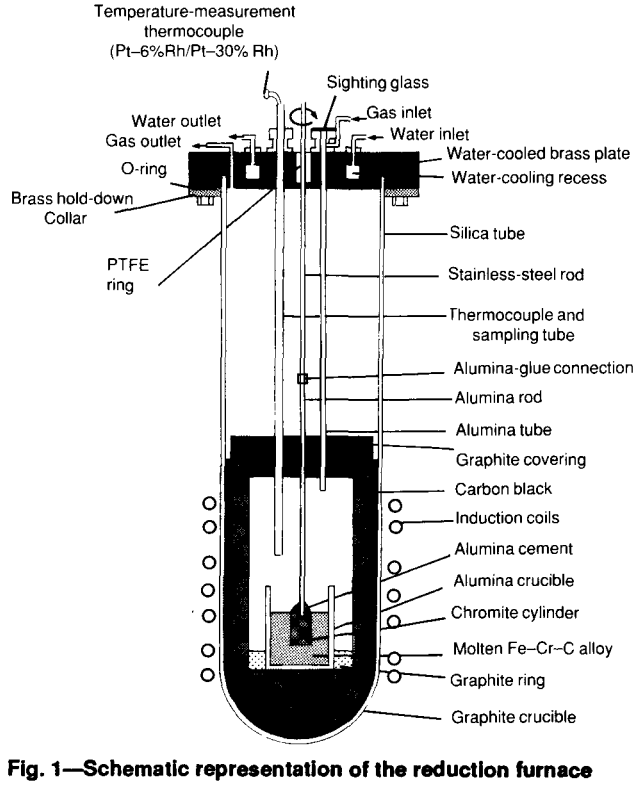

Fig. 1—Schematic representation of the reduction furnace

TABLE I

SCREEN ANALYSIS OF TABLED AND PULVERIZED CHROMITE ORIGINATING FROM THE LG-6 SEAM OF THE BUSHVELD COMPLEX

Sieve size		Retained by sieve %	Σ retained by sieve %	Σ passed by sieve %
Tyler mesh	μm			
Screen analyses of tabled chromite				
48	295	0,000	0,000	100,000
65	208	0,947	0,947	99,053
100	147	3,857	4,804	95,196
150	104	17,239	22,043	77,957
200	74	22,415	44,458	55,542
270	53	24,828	69,286	30,714
400	38	13,335	82,621	17,379
-400	–	17,379	100,00	0,000
Screen analyses of pulverized chromite				
65	208	0,000	0,000	100,000
100	147	0,226	0,226	99,774
150	104	4,101	4,327	95,673
200	74	10,237	14,564	85,436
270	53	11,732	26,296	73,704
400	38	11,956	38,252	61,748
-400	–	61,748	100,000	0,000

TABLE II

ANALYSIS OF THE CHEMICAL CHROMITE (IN PERCENTAGES BY MASS)

Chromite	MgO	Al_2O_3	SiO_2	CaO	TiO_2	Cr_2O_3	Fe_2O_3	FeO
Received	9,148	14,020	0,955	<0,15	0,519	44,940	27,540	18,200
Pulverized	9,645	14,250	0,796	<0,15	0,512	46,330	28,030	17,700
Sintered	9,686	13,475	0,693	<0,15	0,527	46,845	27,580	18,350

TABLE III

ANALYSES OF THE PREMELTED Fe–Cr–C MASTER ALLOYS (IN PERCENTAGES BY MASS)

Alloy	Cr	Fe	Al	Si	C	S	P
1	47,70	49,80	<0,1	<0,2	3,65	0,03	<0,01
2	57,70	35,85	<0,1	<0,2	6,38	0,04	<0,91

through a junction to an alumina inlet tube with an internal diameter of 5 mm. One end of the inlet tube was located 3 cm above the surface of the melt, while the other end was closed at the top by a sighting glass through which the interior of the furnace could be observed.

The chromite-spinel cylinder was rotated at a controlled speed about its long axis by a drive system. The various rotational speeds were obtained from a calibrated variable-speed electric motor, which was connected to the stainless-steel rod by means of a flexible attachment. The rotational speed was checked from readings of a hand-tachometer attached to the shaft of the electric motor. The stainless-steel rod could be raised or lowered by about 6 cm so that the chromite-spinel cylinder could be removed from or immersed in the liquid Fe–Cr–C alloy. Samples were taken with a fused-silica tube (fitted with an aspirator bulb) through the sampling hole, which was otherwise kept closed with the alumina thermocouple-protection tube.

The experimental method basically involved the submersion of rotating chromite-spinel cylinders in a pool of liquid Fe–Cr–C alloy in a pure alumina crucible, and the measurement of changes in the composition of the liquid alloy. The course of the reduction was followed by chemical analysis of the melt in terms of decarburization curves.

In a typical experiment, 200 g of an Fe–Cr–C alloy was charged into the crucible while the cylinder was in its withdrawn position in such a way that the lower tip of the cylinder would be 3 cm above the surface of the liquid metal when the charge had melted. The reaction furnace was sealed and filled with argon gas. As the furnace temperature was raised gradually until the desired level was reached, the cylinder became preheated. After the charge had melted, the thermocouple was immersed in the liquid alloy and kept there until the system reached a steady state at the temperature. The initial sample for chemical analysis was taken by suction, and then the cylinder was

immersed approximately 20 mm into the melt and rotated at the desired speed for specified periods of time. The surface area of the cylinder that was exposed to the molten alloy was 10,14 cm^2, including its bottom surface.

Samples were taken at predetermined time intervals of 15, 30, 60, 120, 180, and 240 minutes. The argon flow was increased during the sampling operation to prevent the entry of air to the furnace chamber.

On completion of a run, the cylinder was raised from the melt and the system was flushed with argon. The metal samples were analysed for carbon, chromium, and iron. Metallographic examination, X-ray-diffraction analyses (XRD), electron-microprobe analyses, and scanning electron-microscope (SEM) analyses were carried out on the reacted samples so that insight could be gained into the mechanism of reduction.

Results and Discussion

The temperature, stirring speed, and composition of the melt were the three main parameters in the reduction of solid chromite in the Fe–Cr–C alloys. These parameters were examined as a function of time.

Decarburization, D, is defined as

$$\%D = (C_i - C_f / C_i) \times 100,$$

where C_i is the initial carbon concentration and C_f is the final carbon concentration of the melt in percentages.

Effect of Temperature

Fig. 2 illustrates the effect of temperature on the carbon content of an alloy initially containing 50 per cent chromium and 6 per cent carbon in contact with the spinel at the optimum rotation of 400 r/min at 1550, 1600, and 1680°C. As the reaction temperature increases, the rate and extent of carbon removal (decarburization), and hence the reduction of the oxide, is increased. This is because higher temperatures favour the decomposition of the oxide and the reduction reaction, both of which are endothermic.

Higher reaction temperatures also result in a higher rate of diffusion of the species, helping the reduction reaction to proceed.

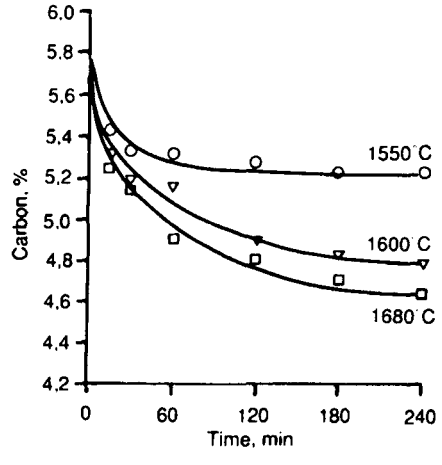

Fig. 2—Effect of temperature on the carbon content of the 50% Cr–6% C alloy at 400 r/min

Effect of Stirring

The effect of the rotational speed of the chromite cylinder on the decarburization of an alloy initially containing 50 per cent chromium and 6 per cent carbon was tested at 1600°C at 100, 200, 400, 600, 800, and 1000 r/min. As the stirring of the melt increased towards 400 r/min, decarburization increased. Thereafter, there was no appreciable effect on the decarburization. The increase in the extent and rate of decarburization was found to be more pronounced in the early stages of reduction. Figs. 3 and 4 illustrate these facts. The decarburization curves obtained for 600, 800, and 1000 r/min finally merged, and were more or less the same as those at 400 r/min.

Although this seems unusual, a similar effect was observed by Barmin *et al.*[8], who studied the rate of the reduction of a chromic oxide disk by carbon in molten iron. In their study, an increase in the rotational speed beyond 570 r/min towards 950 r/min showed no appreciable effect on the decarburization of the alloy. They concluded that, with an increase in rotational speed to 570 r/min, the rate-limiting step in the reaction mechanism changes from mass transfer in the liquid phase to a chemical reaction. A similar phenomenon was observed in the present work: as solid carbides formed around the chromite cylinder, it was likely that the rate-limiting step changed from liquid-phase mass transfer to solid-phase mass transfer.

Composition of the Liquid Alloy

The effect of changes in the chromium content of the melt was tested for alloys containing 4, 5, and 7 per cent carbon at 1500, 1600, and 1680°C respectively. The results of all these experiments showed that, regardless of the temperature and the carbon content of the melt, the

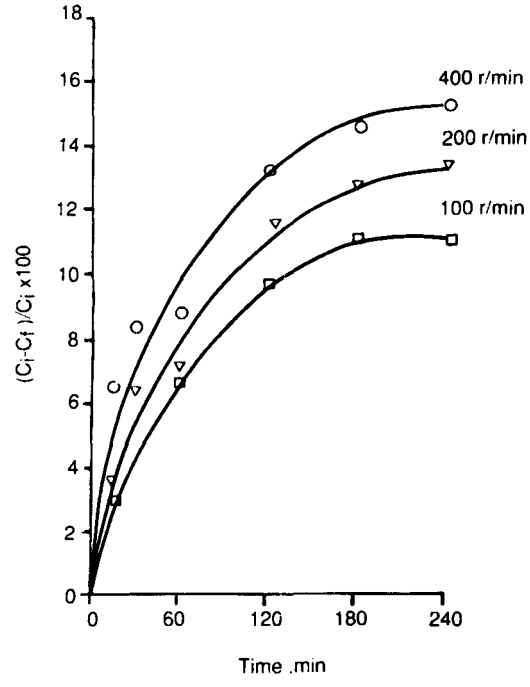

Fig. 3—Effect of stirring on the decarburization of the 50% Cr–6% C alloy at 1600°C and 100, 200, and 400 r/min

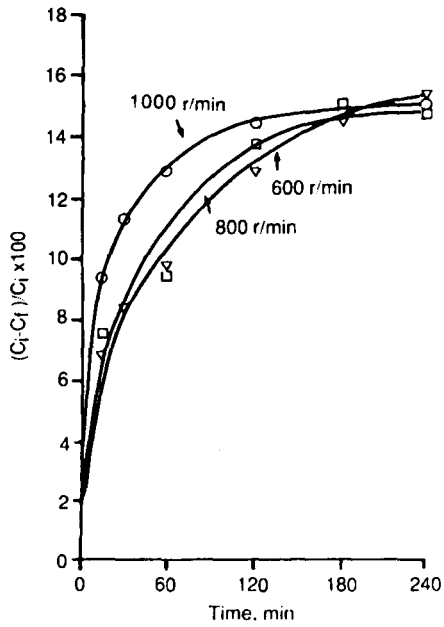

Fig. 4—Effect of stirring on the decarburization of the 50% Cr–6% C alloy at 1600°C and 600, 800, and 1000 r/min

percentage decarburization first increased with an increase in the chromium content in the alloys of up to 50 per cent, and then decreased with a further increase in the chromium content. (Fig. 5). The ratio of the initial to the final carbon activities corresponding to the test compositions, which were taken from the literature[9], first increased with an increase in the chromium content, peaked around a chromium content of 50 per cent, and then decreased; that is, the highest chemical potential difference for carbon was observed around 50 per cent chromium in the alloy. The effect of the activity ratios could be providing the driving force, and hence the high decarburization, at a chromium content of about 50 per cent in the melt.

The set of experiments for alloys containing 50 per cent chromium at 1600°C and 100 r/min revealed that the decarburization increased with an increase in the initial carbon content of the bath (Fig. 6). However, for initial carbon contents of 4 to 8 per cent, the carbon content did not decrease to the equilibrium values that would be expected from thermodynamic principles. This suggests the presence of a possible barrier to the reduction reaction, and hence a possible artificial equilibrium in the melt. That stirring beyond about 400 r/min did not enhance the decarburization is also in accord with this observation.

Microscopic and X-ray-diffraction Analyses

Microscopic examination of a vertical cross-section of the partially reduced chromite cylinders revealed an outer metallized skin, an inner core of more or less unreacted chromite, and a transition zone between the two. Microscopic examination of the outer zone under polarized light indicated the presence of carbides with both cubic and non-cubic morphology.

The outer zones of partially reduced chromite (individually from 15 minutes to 4 hours) reacted at 1600°C in alloys containing 6 per cent carbon and 50 per cent chromium at 400 r/min were examined by XRD analysis. X-ray diffractograms revealed the presence of residual picrochromite and ∝–Fe phase up to about 30 minutes of reaction time, corresponding to 6,5 per cent decarburization. Thereafter, in addition to the above two phases, cubic $M_{23}C_6$ and hexagonal M_7C_3 carbides (M = Cr, Fe) appeared. When the reaction period, and hence the decarburization, increased further, the diffractograms always showed all the above four phases. However, the diffraction patterns of the chromite remained unchanged, although they became progressively weaker. As the reduction progressed, the relative amounts of carbides, especially the M_7C_3 type, increased around the periphery of the chromite cylinder. This also resulted in the retention of the original shape of the cylinder. It appeared that this carbide layer acted as a barrier for further reaction by hindering contact between the alloy and the oxide.

Although the overlapping peaks of ∝–Fe and M_7C_3 made identifications very difficult, all the X-ray analyses were supported by polarized-light microscopy. Carbides with both cubic and non-cubic morphology (with the non-cubic dominating at increased reaction times) were

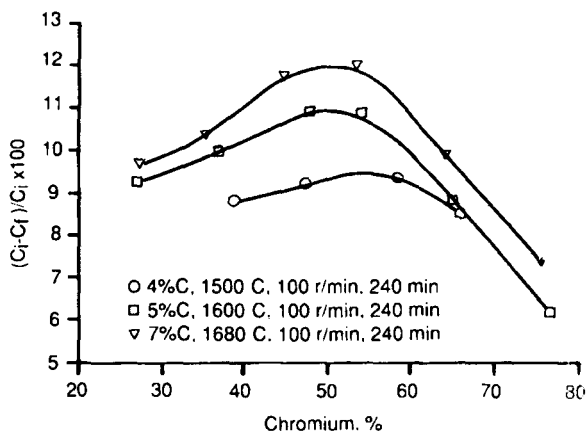

Fig. 5—Effect of initial chromium content on the decarburization of Fe–Cr–C alloys after a reduction time of 240 minutes

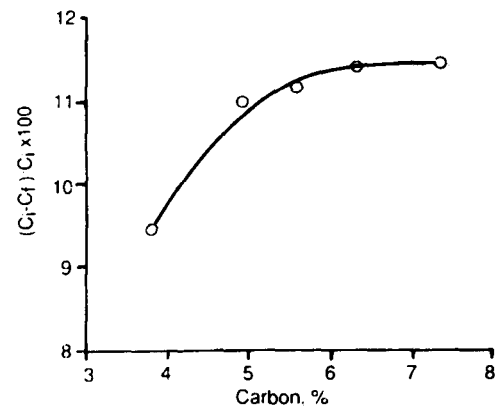

Fig. 6—Effect of initial carbon content on the decarburization of the 50% Cr–6% C alloys at 1600°C and 100 r/min after a reduction time of 240 minutes

observed only after 30 minutes of retention time, supporting the X-ray analysis. In the X-ray studies, great care was taken to avoid samples with admixed bulk alloy. In fact, most of the samples were virtually free of bulk alloy and they were selected more from the interior side of the surface.

The possibility existed that, at the later stages of reduction, the rate-controlling step could be diffusion through this product layer. To test this possibility, a set of experiments was carried out on an alloy containing 6 per cent carbon and 50 per cent chromium. In this set of experiments, a second fresh cylinder of chromite was introduced into the melt that had been used in the first immersion after the first cylinder had been immersed for 4 hours. The results are shown in Fig. 7. It was observed that the decrease in the carbon content of the alloy continued with the immersion of the second fresh cylinder. This demonstrated that there are artificial equilibria in the reduction of chromite spinel, possibly owing to the formation of carbide around the cylinders.

According to Griffing *et al.*'s diagram showing a C–Cr–Fe liquidus surface for carbon 0 to 14 per cent and chromium 0 to 100 per cent, 1600°C is above the liquidus temperature of the alloy containing 6 per cent carbon and 50 per cent chromium. It would be expected that any solid M_7C_3 carbide layer on the surface of the chromite cylinder will have dissolved in the melt. However, the present work showed otherwise. A chromite cylinder was immersed in a liquid alloy containing 6 per cent carbon and 50 per cent chromium at 1600°C, and liquid metallic samples were taken from the melt and quenched immediately in water after a reaction time of 4 hours. Microscopic examination of these samples revealed the presence of M_7C_3 carbide islands in the melt itself as shown in Fig. 8. These carbides were the typical large, angular crystals of a primary phase in the liquid state. It is obvious that the liquid was saturated with respect to carbide at this temperature. Although Griffing *et al.*[10], Jackson[11], and Wethmar[12] report the liquidus temperature for an alloy containing 50 per cent chromium and 6 per cent carbon to be around 1540 ± 20°C, it is possible that there are errors in the reported liquidus surfaces since the temperatures measured in the present study were correct to approximately 10°C. Another potential possibility is the fact that the dissolution rate of these carbides in liquid alloy is extremely slow. The last possibility is the fact that, if the cooling had not been fast enough, these could have been quench crystals. However, the fact remains that the chromite grains were surrounded by carbides.

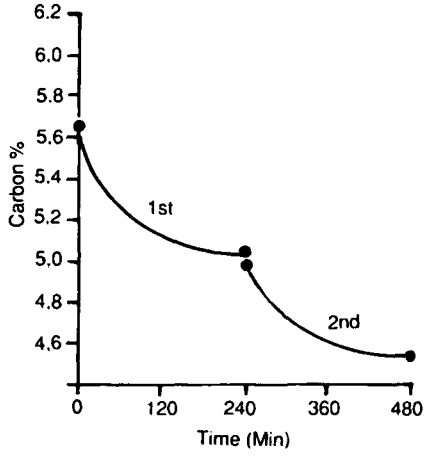

Fig. 7—Decrease in the carbon content of 50% Cr–6% C alloy as a function of time with two consecutively immersed chromite cylinders at 1600°C and 100 r/min

Analysis of the Data

If Al_2O_3, MgO, and TiO_2 are considered to be unreducible oxides in chromite spinel, the reduction of chromite by carbon dissolved in Fe–Cr alloys can be represented by the following consecutive steps.

(1) $FeCr_2O_4$ dissociates at the oxide–metal phase boundary, i.e.

$$FeCr_2O_4(s) = 2\underline{Cr}\ (l) + \underline{Fe}\ (l) + 4\underline{O}\ (\%), \quad [2]$$

where % indicates a standard state of 1,0 per cent by mass.

(2) Chromium, iron, and oxygen are transported from the oxide–metal phase boundary to the bulk metal.

(3) Oxygen and carbon are transported from the bulk metal to the metal–gas phase boundary.

(4) Carbon and oxygen react at this metal–gas phase boundary to form carbon monoxide gas, i.e.

$$\underline{C} + \underline{O}\ (\%) + CO\ (g)\,. \quad [3]$$

(5) Since carbides appeared on the surface of the cylinder after about 30 minutes of reaction time, carbide–metal and carbide–oxide phase boundaries are created at later stages of the reduction. The transport of carbon through the carbide phase or that of carbon monoxide through micro-cracks within the carbide skin is

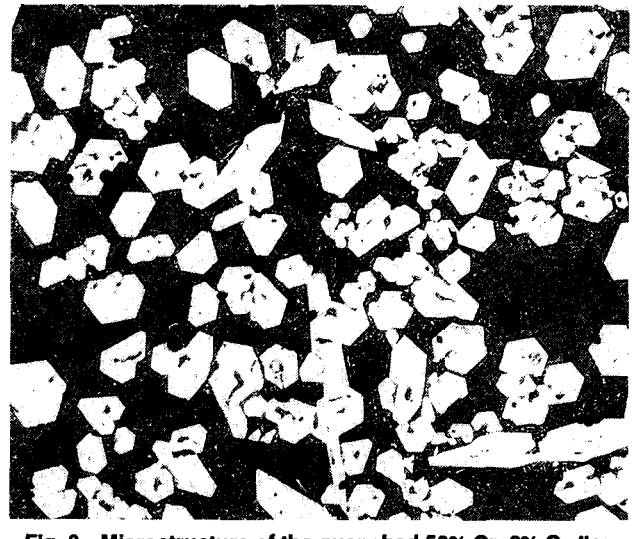

Fig. 8—Microstructure of the quenched 50% Cr–6% C alloy after it had been reacted with the chromite spinel cylinder at 1600°C for 4 hours. The white areas are M_7C_3 carbide. Magnification 100x

possible. On the other hand, the transport of chromium and iron through the oxide phase towards the oxide–carbide phase boundary is another possible step. M_7C_3-type carbide is more stable thermodynamically, and is the dominant phase as evidenced experimentally in this work. Furthermore, the following reaction can be considered for further reduction of the chromite and dissolution of the $M_{23}C_6$ carbide in the solid state at the oxide–carbide phase boundary:

$$FeCr_2O_4(s) + 1{,}65\ (Fe_{16,60}Cr_{6,40})C_6 + 10{,}92\ \underline{C} = 4{,}00\ CO\ (g) + 1{,}701\ Fe + 5{,}607(Fe_{4,76}Cr_{2,24})C_3\ . \qquad [4]$$

The composition of the carbides in reaction [4] is given in averaged values obtained from SEM-EDAX and microprobe analyses of these carbides.

It is assumed that steps [1] and [4] could not be the rate-determining steps because of the high temperature involved[13]. Because the concentrations of chromium and iron in the liquid alloy are high and essentially constant, it is assumed that there are no significant concentration gradients for chromium and iron between the boundary liquid alloy and the bulk liquid alloy. Therefore, the transport of chromium and iron involved in step [2] can be eliminated.

In view of the fact that the rate of reaction is altered by changes in the rotational speed of the chromite cylinder—especially at the initial stage of the reduction—it is presumed that the reduction rate of chromite into the melt is controlled by the mass transfer in the melt at this initial stage. Had the reduction of chromite been chemically controlled, the rate would not have been affected by stirring[13–17].

Step [5], involving a number of stages, will be discussed as a rate-limiting process for the later part of the reduction after a consideration of liquid-phase mass transfer. The thermodynamic data needed for the analysis of these steps are available in the literature[16–23].

Liquid-state Mass Transfer

The evolution of bubbles of carbon monoxide in the vicinity of the oxide–melt interface is considered to alter the oxide–melt and the melt–gas interfacial areas. The mass-transfer coefficients are also altered by the formation of bubbles. However, since the altered values of the interfacial area and the mass-transfer coefficients cannot be evaluated accurately, the rate data are analysed here on the premise that the oxide–melt interfacial area is a constant, A. In every experiment, the evolution of bubbles of carbon monoxide gas was observed at the cylinder–melt interface, and the effect of bubble formation on the mass-transfer rate is therefore shown by the value of the mass-transfer coefficients. If the greater part of the oxygen is converted to carbon monoxide bubbles in the vicinity of the oxide–melt interface, liquid-state mass transfer of oxygen from the bulk liquid metal to the metal–gas phase boundary can be eliminated as a rate-determining step. Hence, the mass transfer of oxygen from the oxide–metal phase boundary to the bulk metal is considered to be as follows.

The rate of decarburization for the oxygen transport can be described by

$$-\frac{d[\%C]}{dt} = \left(\frac{M_c}{M_o}\right)\left(\frac{d[\%O]}{dt}\right) = \left(\frac{M_c}{M_o}\right)\left(\frac{A}{V_m}\right)k_o([\%O_s]-[\%O_b])\ , \qquad [5]$$

where M_c and M_o are the molecular masses of carbon and oxygen respectively, A is the interfacial area, V_m is the volume of the melt, and k_o is the mass-transfer coefficient of oxygen.

The term on the far left gives the rate at which oxygen passes out of the system as carbon monoxide gas, i.e. the rate of decarburization, and the term on the right is the rate at which oxygen passes from the oxide into the liquid metal. The subscripts s, b, and g refer to the oxide–metal interface, bulk-metal interface, and gas–metal interface respectively.

The concentration of oxygen in the bulk metal, $[\%O_b]$, is determined by the carbon–oxygen equilibrium, which is represented by equation [3]:

$$K_3 = P_{co}/a_c f_{og}\,[\%O_g] \qquad [6]$$

where P_{co} is the partial pressure of the carbon monoxide gas, a_c is the activity of the carbon with pure graphite as the standard state, and f_o is the activity coefficient of oxygen in the infinitely dilute reference state with the standard state of 1 per cent by mass. Again, the subscript g refers to the gas–metal interface.

It is to be noted for this case that

$$f_{og} = f_{ob} = f_o \qquad [7]$$

and that

$$[\%O_g] = [\%O_b]. \qquad [8]$$

Therefore,

$$[\%O_b] = [\%O_g] = P_{co}/K_3\,a_c f_o. \qquad [9]$$

The term $[\%O_g]$ is the oxygen content of the liquid in equilibrium with the spinel $FeCr_2O_4$, as defined by equation [2]:

$$K_2 = a_{Cr}^2\,a_{Fe}\,f_o^4\,[\%O_s]^4/a_{FeCr_2O_4} \qquad [10]$$

where f_{os} is assumed to be equal to f_{og} and where ($f_o = f_{ob} = f_{og} = f_{os}$) are the activity coefficients of oxygen in the bulk metal, at the gas–metal interface, and at the oxide–metal interface respectively.

It should be noted that the analysis of the process must account for the fact that the concentrations of carbon, chromium, and iron in the bulk liquid are changing as the reaction proceeds: the carbon decreases, and the chromium and iron increase. Therefore, a_{Cr}, a_{Fe}, (with pure liquid metals as the standard states), and a_c must be expressed in

terms of the concentration in the melt and the appropriate interaction coefficients.

The chemical formula of the natural chromite was estimated to be

$$(Fe^{2+}_{4,03}, Mg^{2+}_{3,97})\,[Cr^{3+}_{10,01}, Al^{3+}_{4,29}, Fe^{3+}_{1,48}, Fe^{2+}_{0,11}, Ti^{4+}_{0,11}]\,O^{2-}_{32},$$

from which the activity of $FeCr_2O_4$ can be calculated, if ideal mixing on atomic sites is assumed, as[24]

$$a_{FeCr_2O_4} = (4,03)\,[10,01]^2/(8)\,[16]^2 = 0,197. \qquad [11]$$

P_{co} is taken to be equal to unity, because gas bubbles surrounding the cylinder would be the reaction product of pure carbon monoxide. The density of the melt, and hence the volume of the melt, was estimated as a function of the temperature and the carbon content of the melt.

Because the length and diameter of the cylinders were the same after the experiments, the reaction site was limited to the cylindrical and bottom surfaces of the cylinder, which were taken to be constant and equal to A.

The solving of equation [10] for $(\%O_s)$ gives

$$\%O_s = \frac{1}{f_O}\,[K_2\, a_{FeCr_2O_4}/a^2_{Cr}\, a_{Fe}]^{1/4}. \qquad [12]$$

The insertion of equations [9] and [12] into equation [5] gives

$$-\frac{d[\%C]}{dt} = \left(\frac{M_o}{M_o}\right)\cdot\left(\frac{A}{V_m}\right)k_o \cdot\left[\frac{1}{f_o}\left(K_2\, a_{FeCr_2O_4}/d^2_{Cr}\, a_{Fe}\right)^{1/4} - \frac{P_{co}}{K_3\, a_c f_o}\right] \qquad [13]$$

The separation of the variables and their integration between the limits gives

$$-\left(\frac{M_o}{M_c}\right)\left(\frac{V_m}{A}\right)\int_{co}^{\%C} \frac{d[\%C]}{\left[\frac{1}{fo}\left(K_2\, a_{FeCr_2O_4}/d^2_{Cr}\, a_{Fe}\right)^{1/4} - \frac{P_{co}}{K_3\, a_c f_o}\right]} = \int_o^t k_o\, dt. \qquad [14a]$$

$$-f\,(oxygen\text{-}transport\ control) = kt. \qquad [14b]$$

A plot of the lefthand side of the equation [14b] versus time should result in a straight line if the reaction is transport-controlled, and if the mass-transfer coefficient, k_o, is constant. The lefthand side of the equation [14a] after integration is referred to as f (oxygen-transport control). This is purely an arbitrary notation, simply indicating the assumption of oxygen-transport rate control. The integral was evaluated numerically by the insertion of the values of K_2, the equilibrium constant for reaction [2] $a_{FeCr_2O_4}$ = 0,197, P_{CO} = 1,0 atm, and K_3, the equilibrium constant for reaction [3]. As indicated earlier, the a_c, a_{Cr}, a_{Fe} and f_o values were evaluated at every experimental point (which is a function of time) using the known compositional data. In the case of f_o, only first-order interaction coefficients were employed. These were then inserted into the integral of equation [14a] for the evaluation of f (oxygen-transport control). The plots are presented in Figs. 9 and 10 for up to 30 minutes of reaction time, where they are linear. The linearity in the figures also indicates that the process is possibly controlled by oxygen transport in this initial stage, and the values of k_o are constant. The mass-transfer coefficients were calculated by linear-regression analyses of the data for 10 to 30 minutes, and are tabulated in Tables IV and V.

TABLE IV
MASS-TRANSFER COEFFICIENT OF OXYGEN AS A FUNCTION OF THE ROTATIONAL SPEED OF THE CYLINDER AT 1600°C

w r/min	k_o x 10^{+6} cm/s	Correlation coefficient r
100	2,279	0,990
200	3,985	0,993
400	5,089	0,994
600	7,103	0,992
800	9,792	0,987
1000	10,232	0,994

TABLE V
MASS-TRANSFER COEFFICIENT OF OXYGEN AS A FUNCTION OF MELT TEMPERATURE AT 400 r/min

T °C	k_o x 10^{+6} cm/s	Correlation coefficient r
1550	4,657	0,989
1600	5,089	0,994
1680	6,716	0,992

As indicated earlier, the other option for rate control is the mass transfer of carbon from the bulk metal to the metal–gas boundary. In order to clarify whether the rate is controlled by oxygen transport or by carbon transport, a similar analysis has to be made for carbon mass transfer so that the results for oxygen transport and carbon transport can be compared.

In the following, the assumption was made that the reaction rate is now controlled by the mass transfer of carbon from the bulk metal to the metal–gas boundary. The rate is then expressed by

$$\frac{d[\%C]}{dt} = -k_c\left(\frac{A}{V_m}\right)\left[\%C_b - \%C_g\right], \qquad [15]$$

where k_c is the mass transfer coefficient of carbon. The values of $[\%C_g]$ could simply be obtained from the relationship $a_c = f_{cg}\,[\%C_g]$ since the activities of carbon were known as a function of melt composition. The activity

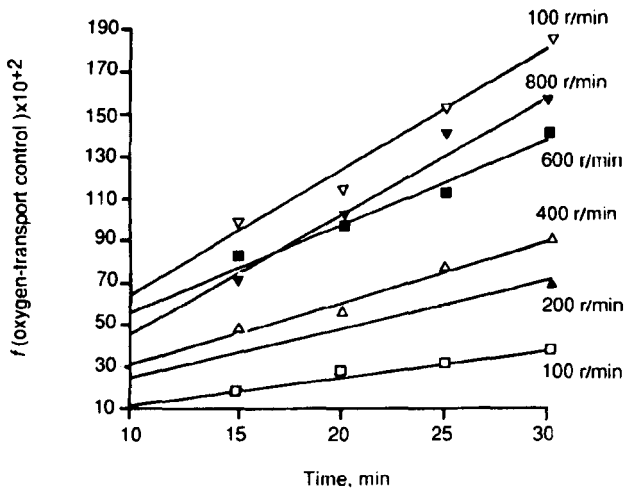

Fig. 9—The use of integrated rate equation [14] to give values of k_o at various rotation rates

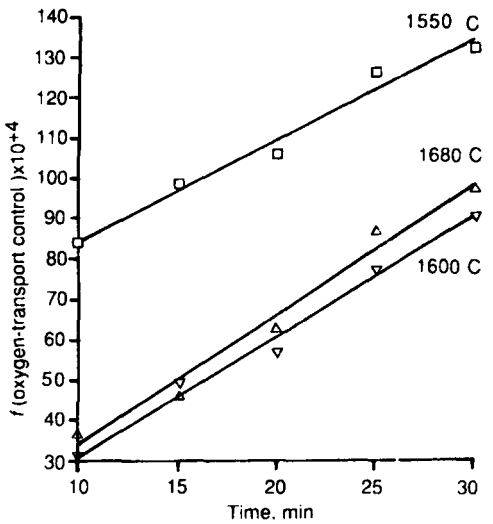

Fig. 10—The use of integrated rate equation [14] to give values of k_o at different temperatures

coefficient of carbon, f_{cg} was easily obtained as a function of melt composition by use of the first-order interaction coefficients available in the literature, thus yielding $[\%C_g]$ values. However, the calculated values of $[\%C_g]$ for appropriate runs were all very small in comparison with $[\%C_b]$ values. Therefore, for the sake of simplicity, the $[\%C_g]$ term in equation [15] was neglected, and the integrated form of equation [15] was written as

$$2{,}303\left(\log[\%C_o]-\log[\%C_o]\right)V_m/A=\int_o^t k_c\,dt. \qquad [16]$$

The lefthand side of equation [16] was given the arbitrary name f (carbon-transport control) and was evaluated from the experimental data where $\%C_o$ is the initial carbon concentration. The relationship between the lefthand side of equation [16] and time is shown in Figs. 11 and 12, again up to 30 minutes of reaction time where linearity exists. The mass-transfer coefficients of carbon obtained in a similar way to the mass-transfer coefficients of oxygen by linear regression of the plotted data are listed in Tables VI and VII.

Nevertheless, the liquid-phase mass-transport coefficients for oxygen and carbon as obtained above do not reveal which of the two is responsible for rate control. This

TABLE VI
MASS-TRANSFER COEFFICIENT OF CARBON AS A FUNCTION OF THE ROTATIONAL SPEED OF THE CYLINDER AT 1600°C

w r/min	k_o x 10^{+5} cm/s	Correlation coefficient, r
100	5,207	0,983
200	7,923	0,986
400	9,967	0,987
600	11,100	0,988
800	14,940	0,980
1000	15,383	0,993

TABLE VII
MASS-TRANSFER COEFFICIENT OF CARBON AS A FUNCTION OF MELT TEMPERATURE AT 400 r/min

T °C	k_o x 10^{+5} cm/s	Correlation coefficient, r
1550	5,033	0,993
1600	9,967	0,987
1680	14,317	0,996

is analysed in the next section of this paper. However, after 30 minutes of reaction time, non-linearity is observed for both sets of coefficients, indicating a switch in rate processes, i.e. liquid-phase mass transport is not the rate-controlling mechanism after 30 minutes. This is a result of the proximity of the system to artificial equilibrium, i.e. the apparent area of contact between the oxide and the liquid metal is decreasing because of the formation of the solid carbides M_7C_3 and $M_{23}C_6$ on the surface of the cylinder. Solid-state processes are important for further reduction.

Mass Transfer of Oxygen and Carbon

In several studies in which rotating cylinders were used, the mass-transfer coefficient was found to depend on rotational speed (w) according to a power function[13,17].

$$k = constant\ (w)^n. \qquad [17]$$

The plots of logarithms k_o and k_c versus logarithm w were constructed. The regression analyses of the present experimental data gave the values of n as 0,62 and 0,46 for oxygen and carbon respectively. For rotating cylinders, the mass-transfer coefficient is a function of the Schmidt (Sc), and Reynolds (Re) numbers. Eisenberg and his coworkers[25] obtained

$$k = 0{,}0791\ Sc^{-0{,}644}Re^{0{,}30}U, \qquad [18]$$

and Kim and Pehlke[26] found

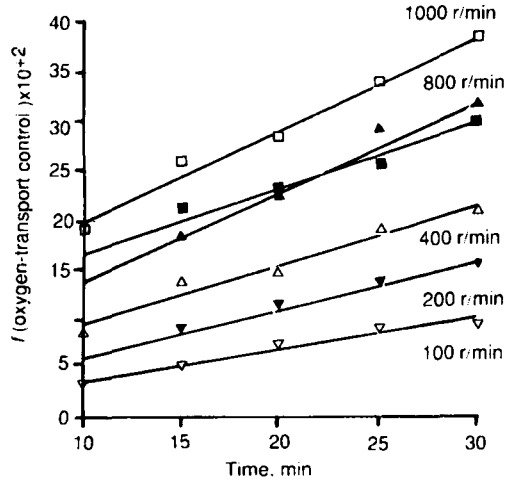

Fig. 11—The use of integrated rate equation [16] to give values of k_c at various rotation rates

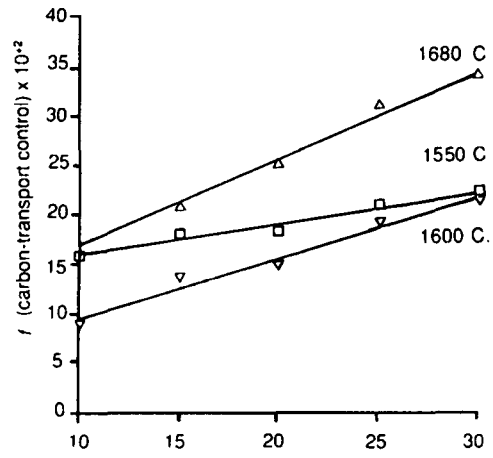

Fig. 12—The use of integrated rate equation [16] to give values of k_c at various temperatures

$$k = 0{,}112\, Sc^{-0{,}644} Re^{0{,}33} U, \qquad [18]$$

where $Re = dU\rho/\mu = Ud/\nu$

$Sc = \mu/\rho D$

d = Diameter of cylinder, cm

w = Rotational speed, s^{-1}

ρ = Density of melt, g/cm^3

μ = Viscosity, P

ν = Kinetic viscosity (μ/ρ), cm^2/s

U = Peripheral velocity ($\pi dw/60$), cm/s

D = Diffusion coefficient, cm^2/s.

For the present case, similar equations for the mass-transfer coefficients of carbon and oxygen based on Schmidt and Reynolds numbers can be developed as follows:

$$k = \text{constant}\, Sc^{-0{,}644} Re^{-m} U. \qquad [19]$$

The insertion of $U = \pi dw/60$, $Sc = \mu/\rho D$, and $Re = Ud/\nu$ into equation [19] gives

$$k = \text{constant}\, (\pi/60)^{1-m} d^{1-2m} \nu^{m-0{,}644} D^{0{,}644} w^{1-m}. \qquad [20]$$

A comparison of equation [20] with equation [17] (where n was 0,46 for carbon and 0,62 for oxygen) gives values for m of 0,54 for carbon and 0,38 for oxygen respectively. These are used later in the calculation of activation energies.

At the optimum rotational speed of 400 r/min, the mass-transfer coefficients k_o and k_c were determined at 1550, 1600, and 1680°C by linear-regression analyses of the data for the initial stage of the reduction. These were plotted against $1/T$. The regression analyses of the plots show that the apparent activation energies of decarburization are 84,864 kJ per mole of oxygen and 229,747 kJ per mole of carbon.

On the other hand, the temperature dependence of k_o and k_c can be calculated by use of equation [20] coupled with the data for the activation energies for diffusion and viscous flow. The differentiation of the logarithm of equation [20] with respect to $1/T$ results in

$$\frac{d \ln k}{d(1/T)} = (m - 0{,}644)\frac{d \ln \nu}{d(1/T)} + 0{,}644 \frac{d \ln D}{d(1/T)}. \qquad [21]$$

In accordance with the usual Arrhenius-type temperature dependence of the mass-transfer coefficient, viscosity, and diffusivity,

$$k = k^{\circ} \exp [-Q_k/RT], \qquad [22]$$

$$\nu = \nu^{\circ} \exp [+Q_\nu/RT], \qquad [23]$$

and

$$D = D^{\circ} \exp [-Q_D/RT]. \qquad [24]$$

Equation [21] can be written as

$$Q_k = (0{,}644 - m)\, Q_\nu + 0{,}644\, Q_D. \qquad [25]$$

The following activation energies are given in the literature:

Q_v for Fe–50% chromium alloys[27] ≈ 14,34 kcal/mol

Q_v for Fe–C alloys[28] = 10,2 ± 0,9 kcal/mol

Q_D for carbon[29] = 13,8 ± 0,8 kcal/mol

Q_D for carbon[30] = 10 kcal/mol

Q_D for oxygen[31] = 19,5± 0,75 kcal/mol.

When use is made of Q_v = 12,3 kcal/mol, Q_D = 19,5 kcal/mol for oxygen, and Q_D = 11,9 kcal/mol for carbon (which are averaged values), the temperature dependence of the mass-transfer coefficients for oxygen and carbon can be expressed as

Q_{ko} = (0,644-0,380) 12,3 + 0,644 (19,5)=15,81 kcal per mole of oxygen

= 66,14 kJ per mole of oxygen

Q_{kc} = (0,644-0,540) 12,3 + 0,644 (11,9) =8,94 kcal per mole of carbon

= 37,42 kJ per mole of carbon.

Because the experimental and calculated activation energies for carbon differ considerably, it is very unlikely that

the transport of carbon controls the rate of reduction of chromite. If the various assumptions made in the determination of the mass-transfer coefficients are taken into consideration, the agreement between the experimental and the calculated activation energies (84,86 kJ and 66,14 kJ respectively) for oxygen is regarded as fairly good. Therefore, it is most likely that the reduction of chromite by carbon dissolved in liquid Fe–Cr alloys is rate-limited by the transport of oxygen at the oxide–metal phase boundary in the initial stage of reduction.

Solid-state Mass Transfer

Rankin[3,32] studied the reduction sequence of chromite from the Bushveld Complex in the solid state by use of both graphite and carbon monoxide gas. His work showed zoning in the particle, and clearly demonstrated the outward diffusion of iron within the particle. The zoning in reacted chromite particles was observed by Kinloch[33], Searle and Finn[4], and Soykan[34]. A number of reduction mechanisms at different temperatures between 1300 and 1416°C were proposed for solid-state reduction [24,33]. In these mechanisms, the spinel phase was assumed to remain stoichiometric as the reduction proceeded [24,34].

In the present study, the main reduction temperature was 1600°C, approximately 200°C higher than the nearest temperature in solid-state work. It can be expected that the assumption of stoichiometry of the spinel phase is no longer valid. In this work , the concentration profiles for chromium, iron, aluminium, magnesium, and titanium were constructed for partially reduced chromite grains by line scans with a SEM–EDAX combination. These analyses were done on samples reacted individually for 15, 30, 60, 120, 180, and 240 minutes. For each reaction time, three samples of the reacted chromite cylinders were examined: one from the outer metallized zone, one from the inner centre zone, and one from the transition zone (between the inner and outer zones). Examples of the scans are given in Figs. 13 and 14. No consistent results were achieved with respect to cation distributions and the stoichiometry of the spinel. However, concentration gradients were observed particularly for chromium and iron in grains at the transition zone, indicating outward diffusion of these species.

Electron-microprobe analyses were also carried out on the chromite grains and the metallized regions taken from the inside of the reacted chromite cylinders. A typical result is summarized in Table VIII.

The results of Table VIII confirm that the metallized regions situated towards the interior of the cylinder are

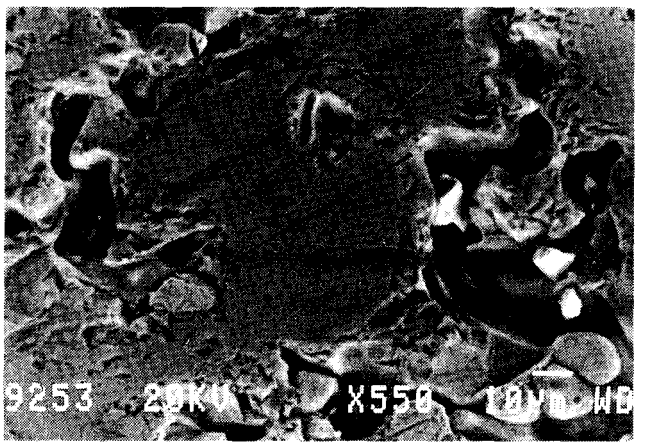

Fig. 13—Second electron image of a grain taken from the transition zone of the chromite cylinder reduced in an alloy of 50Cr–44% Fe–6%C at 1600°C and 400 r/min for 4 hours

composed mainly of iron. The reason for this is quite clear: as the reduction proceeds, the chromite grains are depleted in iron owing to the higher reducibility of ferrous oxide than that of chromic oxide[35].

The lack of diffusion of carbon through the chromite grains shows that carbon monoxide gas can be considered to be the reductant that is responsible for the metal islands observed inside the cylinder. Metallization occurs through micro-cracks inside the chromite cylinders. As these cracks are inaccessible to carbon in the liquid metal and carbon in the carbide, only the carbon monoxide gas can be responsible for the metallization within the cracks, where the nucleation of metal would be easiest owing to the low surface energy.

Finally, chromium also reports to the metallized regions. These results agree with the results obtained by Lisniak and Slecev[36], who state that metallic iron catalyses the reduction of chromic oxide in the chromite spinel, and that metallization of chromium becomes significant with an increase in the extent of reduction.

In the double carbide $(Fe, Cr)_7C_3$, the theoretical mass of carbon can vary between 8,4 and 9,0 per cent according to the relative amounts of iron and chromium present. Iron and chromium in the metal phase formed at the surface of the chromite cylinder were analysed by EDAX. The averaged value for iron was found to be 63,564 per cent and for chromium 27,777 per cent. When carbon was calculated by subtraction, an average of 8,659 per cent was obtained, which is very close to the 8,7 per cent average carbon value of the carbide. Consequently, the chemical formula of this carbide can be written as $(Fe_{4,76}\ Cr_{2,24})C_3$.

TABLE VIII
ELECTRON-MICROPROBE ANALYSES OF THE METALLIC AND OXIDE REGIONS IN THE INTERIOR OF A CHROMITE CYLINDER REACTED FOR 4 HOURS

	C	Mg	Al	Cr	Fe	Total
Metal	3,7417	0,0029	1,1584	19,8586	75,8390	100,6006
	4,1304	0,0072	1,1747	19,8746	75,3728	100,5597
	O	MgO	Al_2O_3	Cr_2O_3	FeO	Total
Oxide	34,8356	14,4040	17,0775	64,3077	3,4613	99,2506
	35,1365	12,6637	19,9454	64,0534	2,2137	98,8761

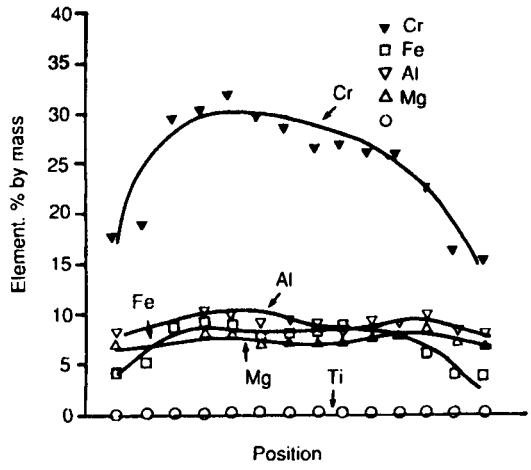

Fig. 14—Variations in elemental concentrations across the grain shown in Fig. 13

When the present experimental data were analysed by classical diffusion models[37], the carbon percentages determined experimentally were converted into percentage reduction by use of reaction [4], which takes into account both the double carbides, the reduction of chromite, the dissolved carbon (thus its diffusion), and the products such as iron and carbon monoxide (thus their transport). It must be noted that, towards the interior of the particle, the metallized regions are essentially iron as substantiated by EDAX studies. The following equation of Zhuravlev, Lesokhin, and Tempel'man[38] was found to fit the data after 30 minutes of reaction time reasonably well:

$$k_{zlt}\, t = 2kDt/r_o^2 = [(1/(1-R)^{1/3}-1]^2. \qquad [26]$$

Within the initial 30 minutes of reaction time, liquid mass transfer of oxygen was already found to be the most likely rate-determining step. In equation [26], k_{zlt} is the Zhuravlev, Lesokhin, Tempel'man rate constant, t is time, k is the rate constant, D is the diffusion coefficient, r_o is the initial radius of the particles, and R is the fraction of the reaction completed (in this work corresponding to the reduction fraction, i.e. the mass of oxygen removed/the mass of removable oxygen). The application of equation [26] is shown in Fig. 15. From equation [26] and Fig. 15, the rate constant, k_{zlt} , for temperatures 1550, 1600, and 1680°C were calculated by linear regression. The values are tabulated in Table IX.

TABLE IX
CALCULATED RATE CONSTANTS AS A FUNCTION OF TEMPERATURE

Temperature °C	Rate constant (k_{zlt})	Correlation coefficient (r)
1550	1,096 x 10^{-5}	0,9972
1600	3,652 x 10^{-5}	0,9914
1680	9,125 x 10^{-5}	0,9972

The relationship between the rate constant and the temperature is usually expressed in an Arrhenius form:

$$k = Ae^{-Q/RT}, \qquad [27]$$

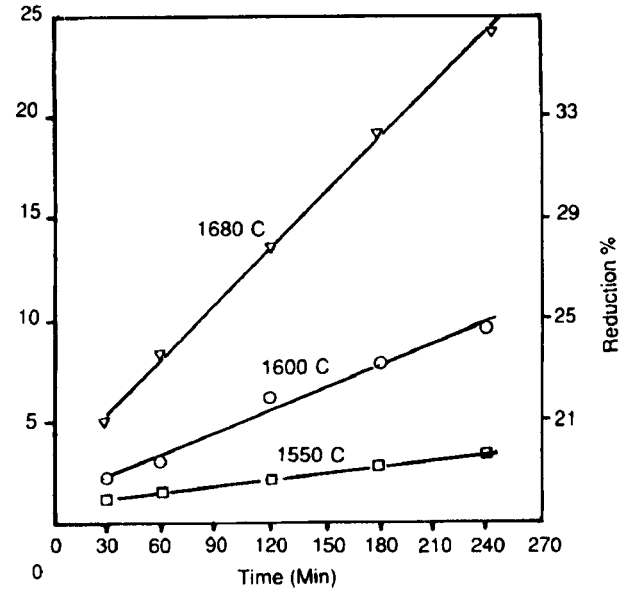

Fig. 15—Schematic representation of the application of Zhuravlev, Lesokhin, and Tempel'man's equation to the experimental data

where R is the universal gas constant, and A is the pre-exponential factor. When $\ln k$ versus $1/T$ is plotted, the activation energy Q is obtained. The apparent activation energy for the diffusion in the solid state determined in the present case was 471,18 kJ/mol.

This energy barrier is rather high for the diffusion of carbon through the carbide layer into the oxide–carbide interface. In view of the much larger radii of iron and chromium atoms when compared with that of carbon atoms, it can be concluded that the outward diffusion of iron and/or chromium in the oxide phase is the most likely rate-determining step in this solid-state process. The concentration gradients observed for iron and chromium from the transition zone of the chromite cylinder (Fig. 14) firmly support this. The above value of activation energy compares very favourably with the value of 468,61 kJ/mol for the diffusion of Fe^{3+} in Fe_2O_3. It should be mentioned that the present analysis does not isolate the actual rate-determining step, and thus the diffusing species.

Conclusion

In the light of the experimental results, the microscopic examination, and the SEM, EMPA, and XRD analyses, a multistage reaction mechanism can be proposed for the reduction of a natural chromite at 1600°C by carbon dissolved in liquid Fe–Cr alloy.

(1) Initially, the reduction of the iron oxides in the spinel starts with the formation of α-iron at surface defects such as micro-cracks. As the reaction proceeds, the reduction of iron oxides to iron continues, but now chromium oxide also begins to be reduced. At this early stage of the reduction, up to about 30 minutes of reaction time, oxygen transport in the liquid alloy at the oxide–melt interface is found to be the most likely rate-determining step.

(2) As a result of the formation of double carbides of the type $(Fe, Cr)_7C_3$ and $(Fe, Cr)_{23}C_6$ on the surface of the chromite cylinder, a change in reduction mechanism occurs after 30 minutes of reaction time in the later stages of the reaction. The direct contact between the oxide and the carbon in the liquid metal is hindered by this growing layer of outer metallized skin, and an artificial equilibrium is reached. It is possible that reduction starts at the interface between the chromite and the liquid alloy, and spreads inwards from this interface by a mechanism involving carbon transfer from the liquid alloy to the chromite grains across the skin of the metallized carbide. Further reduction can occur only by the diffusion of carbon into the oxide through this metallized skin and/or by the diffusion of carbon monoxide gas as a reaction product through micro-cracks in this surface product layer. The outward diffusion of iron and/or chromium in the oxide phase is the most likely rate-determining step in this solid-state reduction region.

The switch from liquid-phase mass transfer to solid-state processes is important since it leads to poor reaction rates and poor recoveries at high temperatures. The interaction of solid chromite with the carbon-containing metal phase is relevant to ferrochromium refining and to the making of stainless steel. It is therefore recommended that a more intensive investigation of this phenomenon should be conducted, and a means should be found to minimize the above-mentioned diffusional type of solid-state processes.

Acknowledgements

This paper is published by permission of Mintek. The financial support provided by Mintek and the Ferro Alloy Producers' Association is gratefully acknowledged.

References

1. BARCZA, N.A. Studies of incipient fusion in the system chromite $-Al_2O_3-C$. Johannesburg, National Institute for Metallurgy, *Report* 1356. Jan. 1972.
2. WOOLLACOTT, N.L. Factors affecting the carbon contents of the alloys formed during the prereduction of chromite ores. Randburg, National Institute for Metallurgy, *Report* 1950. Mar. 1978.
3. RANKIN, W.J., and FINN, C.W.P. Solid-state reduction by graphite and carbon monoxide of chromite from the Bushveld Complex. Randburg, National Institute for Metallurgy, *Report* 1957. May 1978.
4. SEARLE, M.J., and FINN, C.W.P. The mathematical modelling of the reduction behaviour of chromite from the Upper Chromitite Layer of the Bushveld Complex. Randburg, Mintek, *Report* M96. Jul. 1983.
5. KUCUKKARAGOZ, C.S., ALGIE, S.H., and FINN, C.W.P. Reduction of Winterveld chrome spinel at 1300° under an argon atmosphere in the presence of carbon. Randburg, Mintek, *Report* M154. Oct. 1984.
6. ALGIE, S.H., and FINN, C.W.P. Reaction mechanism in the reduction of Winterveld chrome spinel with graphite and carbon under an argon atmosphere at 1300°C. Randburg, Mintek, *Report* M157. Dec. 1984.
7. DE WAAL, S.A., and HIEMSTRA, S.A. The mineralogy, chemistry, and certain aspects of reactivity of chromite from the Bushveld Igneous Complex. Johannesburg, National Institute for Metallurgy, *Report* 1709. Apr. 1975.
8. BARMIN, L.N., *et al.* Kinetics of reduction of solid Cr (III) by carbon dissolved in Fe. Izvetiya Vysshikh Uchebnykn Zaveden, *Chemica metallurgiya*, vol. 11, no. 8. 1968. pp. 20–23.
9. HEALY, G.W. Activities in liquid Cr–Fe–C system above 1600°C. *Proceedings of Reinhardt Schumann International Symposium on Innovative Technology and Reactor Design in Extractive Metallurgy.* TSM-AIME Fall Meeting for Extraction and Process Metallurgy, Colorado Springs (USA), 1986. pp. 667–679.
10. GRIFFING, N.R., FORGENT, W.D., and HEALY, G.W. C–Cr–Fe liquidus surface. *Trans. Metall. Soc.* AIME, vol. 224. 1962. pp. 148–159.
11. JACKSON, R.S. *ISIJ*, vol. 208, no. 2. 1970. pp. 163–167.
12. WETHMAR, J.C.M. Phase equilibria in the Cr–Fe–Si–C system in the composition range representative of high-carbon ferrochromium alloys produced in South Africa. Johannesburg, National Institute for Metallurgy, *Report* 1457. 1972. 7 pp.
13. SEVINC, N., and ELLIOTT, J.F. Kinetics of reduction of Cr_2O_3(s) by liquid Fe–Cr–C alloys. *Ironmaking and Steelmaking*, no. 5. 1976. pp. 268–278.
14. FRUEHAN, R.J. Rate of reduction of Cr_2O_3 by carbon and carbon dissolved in liquid iron alloys. *Metall. Trans.*, vol 8B. 1977. pp. 429–433.
15. SJOVAL, P. *Proceedings of the Second Japan–Sweden Joint Symposium on Ferrous Metallurgy.* Tokyo, ISIJ, 1978. Cited in Ref. 17.
16. SUZUKI, K., and MORI, K. Rate of reduction of Cr_2O_3 by carbon dissolved in liquid Fe–Cr alloys. *Trans. ISIJ*, vol. 20. 1980. pp. 607–613.
17. KAWAKAMI, M., KITAJIMA, Y., HASHIMOTO, K., and ITO, K. Kinetic study on the smelting reduction of bottom-injected chromite ore powder by dissolved carbon in iron melt. *Trans. ISIJ*, vol. 27, no. 3. 1987. pp. 176–184.
18. *'SEIKOHANNO-NO-SUISHOHEIKOCHI', the 19th Comm. (Steelmaking).* Tokyo, Japan Society for the Promotion of Science, 1984. p. 83.
19. ELLIOTT, J.F. *Electric Furnace Steel Conference Proceedings*, vol. 32. 1974. p. 62.
20. SIGWORTH, G.K., and ELLIOTT, J.F. *Metal Sci.*, vol. 8, 1974. p. 298.
21. GASKELL, D.R. *Introduction to metallurgical thermodynamics.* 1973. p. 501.
22. KUBASCHEWSKI, D., and ALCOCK, C.B. *Metallurgical thermo-chemistry. International Series on Materials Science and Technology.* 5th edition. Pergamon Press, vol. 24. 1979. pp. 280–281.
23. *'SEIKOHANNO-NO-SUISHOHEIKOCHI', the 19th Comm. (Steelmaking).* Tokyo, Japan Society for the Promotion of Science, 1984, p. 49.
24. PERRY, K.P.D. Ph.D. thesis, University of the Witwatersrand, Johannesburg, 1986. 133 pp.
25. EISENBERG, M., TOBIAS, C.W., and WILKE, C.R. *Mass transfer at rotating cylinders. Chem. Eng. Prog. Symp. Ser.*, vol. 51, no. 16. 1955. pp. 1–6.
26. KIM, Y., and PEHLKE, R.D. Mass transfer during dissolution of a solid into liquid in the iron–carbon systems. *Metall. Trans.*, vol. 5. 1974. pp. 2527–2532.
27. PAVARS, I.A., BAUM, B.A., and GEL'D, P.V. Kinematic viscosity and electrical resistance of molten iron–chromium alloys. *Russ. J. Phys. Chem.*, vol. 43, no. 11. 1969. pp. 1542–1545.
28. BARFIELD, R.N., and KITCHENER, J.A. The viscosity of liquid iron and iron–carbon alloys. *J. Iron Steel Inst.*, vol. 180. 1955. pp. 324–329.
29. KAIBICHEV, A.V., and LEPINSKIKH, B.M. Effect of carbon concentration on its diffusion coefficient in liquid iron. *Russ. Metall. (Metal)*, no. 6. 1970. pp. 50–54.
30. MORGAN, D.W., and KITCHENER, J.A. Solutions in liquid iron. *Trans. Faraday Soc.*, vol. 50. 1954. pp. 51–60.
31. MORI, K., and SUZUKI, I. Diffusion of oxygen in liquid iron. *Trans. ISIJ Soc.*, vol. 12. 1972. pp. 464–471.
32. RANKIN, W.J. The composition and structure of chromite during reduction with carbon. *Arch. Eisenhuttenwes.*, vol. 50, no. 9. 1979. pp. 373–378.
33. KINLOCH, E.D. The role of mineralogy in pilot plant prereduction of chromite ores in South Africa. *1st International Congress on Applied Mineralogy.* Johannesburg, Geological Society of South Africa, 1983. pp. 337–349.
34. SOYKAN, O. Ph.D. thesis, University of the Witwatersrand, Johannesburg, 1988.
35. TANEKA, S., and ROBERTSON, D.G.C. Reaction kinetics of friable chromites between 1350 and 1750°C. *Pyrometallurgy '87.* London, Institution of Mining and Metallurgy, 1987. pp. 937–976.
36. LISNIAK, S.A., and SLECEV, N.F. *Sbornik Nauch. Tekhn, Tr. Nouchnissled*, vol. 4, no. 4. 1961. pp. 3–11 (NIM Tr. no. 7078).
37. USLU, E. M.Sc (Eng.) thesis, University of the Witwatersrand, Johannesburg, 1989.
38. ZHURAVLEV, V.F., LESOKHIN, I.G., and TEMPEL'MAN, R.G. *J. Appl. Chem. USSR*, vol. 21, no. 9. 1948. pp. 887–890.